Proc. Natl. Acad. Sci. USA
Vol. 87, pp. 2818–2822, April 1990
Biophysics

Solution conformations of the B-loop fragments of human transforming growth factor α and epidermal growth factor by ^{1}H nuclear magnetic resonance and restrained molecular dynamics

(peptide conformation)

KYOU-HOON HAN*, JIA-LIN SYI†‡, BERNARD R. BROOKS†, AND JAMES A. FERRETTI*

*Laboratory of Chemistry, National Heart, Lung, and Blood Institute, and †Division of Computer Research and Technology, National Institutes of Health, Bethesda, MD 20892

Communicated by F. A. Bovey, December 15, 1989

ABSTRACT **A restrained molecular dynamics simulation approach that explicitly includes the effect of the surrounding solvent molecules is applied to the NMR determination of the conformations of the B-loop fragments of human transforming growth factor α and epidermal growth factor. Backbone interproton distance restraints are obtained by using two-dimensional rotating frame nuclear Overhauser effect spectroscopy (ROESY). The simulations are carried out both in "vacuum" and in "water." The results are discussed in terms of the energetics, agreement with the NMR distances, and the flexibility of the peptides.**

Peptides are receiving considerable attention as a class of pharmaceuticals (1), as models for studying receptor binding domains of proteins (2–6), and as antigens in vaccine development (7). Significant efforts are being made to determine peptide conformations as well as to understand the relationship between conformation and biological function (4, 5, 8).

Various approaches, such as x-ray crystallography (9), circular dichroism spectropolarimetry (10), theoretical prediction methods (11), and NMR spectroscopy (12), provide conformational information on peptides and proteins. However, only NMR spectroscopy provides specific internuclear distance restraints in solution. These restraints are commonly obtained as interproton distances from nuclear Overhauser effect (NOE) or cross-relaxation experiments (13). However, the technique is usually limited to the measurement of interproton distances ≤ 4 Å. This limitation can result in ambiguities in the determination of structures exclusively from the NMR distance restraints. Thus, it is important to supplement these distance measurements with molecular modeling calculations.

Internuclear distances obtained from NMR spectra have often been used as input for distance geometry (14) or energy minimization (15) algorithms to obtain refined low-energy structures. However, such calculations may lead to structures associated with local energy minima. Restrained molecular dynamics simulation combined with energy minimization provides an alternative strategy that in principle can yield a global minimum solution to the conformational problem (16–19). Molecular dynamics simulations use classical mechanics and involve integration of Newton's equations of motion for a suitably prepared system—i.e., it is necessary to integrate the equations

$$\frac{\partial^2 x_i}{\partial t^2} = -\frac{\nabla E(x_i)}{m_i}$$

for all atoms in the system.

The publication costs of this article were defrayed in part by page charge payment. This article must therefore be hereby marked "*advertisement*" in accordance with 18 U.S.C. §1734 solely to indicate this fact.

The explicit inclusion of solvent effects in simulations of proteins and DNA fragments has led to significant improvements in the results (20, 21). Since peptides can adopt different conformations depending on solvent conditions (22), it is necessary to include such effects into any detailed conformational computation. The incorporation of solvent in the restrained molecular dynamics simulations by multiplying the electrostatic term by a $1/r$ screening potential has been reported (16). A unique feature of our study is the explicit inclusion of solvent molecules in the restrained (by NMR distances) molecular dynamics simulations.

We present here the NMR determination of the solution conformations of two cyclic peptide fragments of human epidermal growth factor (hEGF) and human transforming growth factor α (hTGF-α). These peptides are the corresponding B-loop fragments, [Ala^{21}]hTGF-α-(16–32) (Cys-Phe-His-Gly-Thr-Ala-Arg-Phe-Leu-Val-Gln-Glu-Asp-Lys-Pro-Ala-Cys, designated TB) and [Ala^{20}]hEGF-(14–31) (Cys-Leu-His-Asp-Gly-Val-Ala-Met-Tyr-Ile-Glu-Ala-Leu-Asp-Lys-Tyr-Ala-Cys, designated EB). The present study uses 25 randomly generated initial structures for calculations rather than starting with a limited set of structures or with the x-ray coordinates.

MATERIALS AND METHODS

NMR Distance Restraints. To estimate internuclear distances, two-dimensional ROESY [rotating-frame NOE spectroscopy (NOESY)] spectra of TB and EB are obtained on an XL-300 spectrometer with an attenuated transmitter output (4) at several different mixing times. The attenuation was sufficient to minimize effects due to through-bond magnetization transfer. The ROESY method is used instead of NOESY to avoid the "zero-NOE crossing" problem, common for small molecules such as peptides (4, 5, 13) in the M_r 1000–3000 range. Application of improved versions (23) of the original ROESY technique (24) indicates that contribution from the other types of coherence transfer to the cross-peak intensity is not significant at a mixing time >100 ms for peptides.§ Shown in Fig. 1 are the ROESY spectra for TB and EB obtained at 120-ms mixing time, representing the NH–aliphatic regions. For both peptides, strong sequential cross-peak intensities between backbone amide NH and C$^\alpha$H

Abbreviations: NOE, nuclear Overhauser effect; NOESY, NOE spectroscopy; ROESY, two-dimensional rotating-frame NOESY; hEGF, human epidermal growth factor; hTGF-α, human transforming growth factor α; TB and EB, B-loop fragments of hTGF-α and hEGF, respectively.

‡Present address: Advanced Scientific Computing Laboratory, National Cancer Institute, Frederick Cancer Research Facility, Frederick, MD 21701.

§Han, K., *Rotating-Frame NOE of Linear Peptides*, 29th Experimental Nuclear Magnetic Resonance Conference (Varian User's Meeting), April 16, 1988, Rochester, NY.

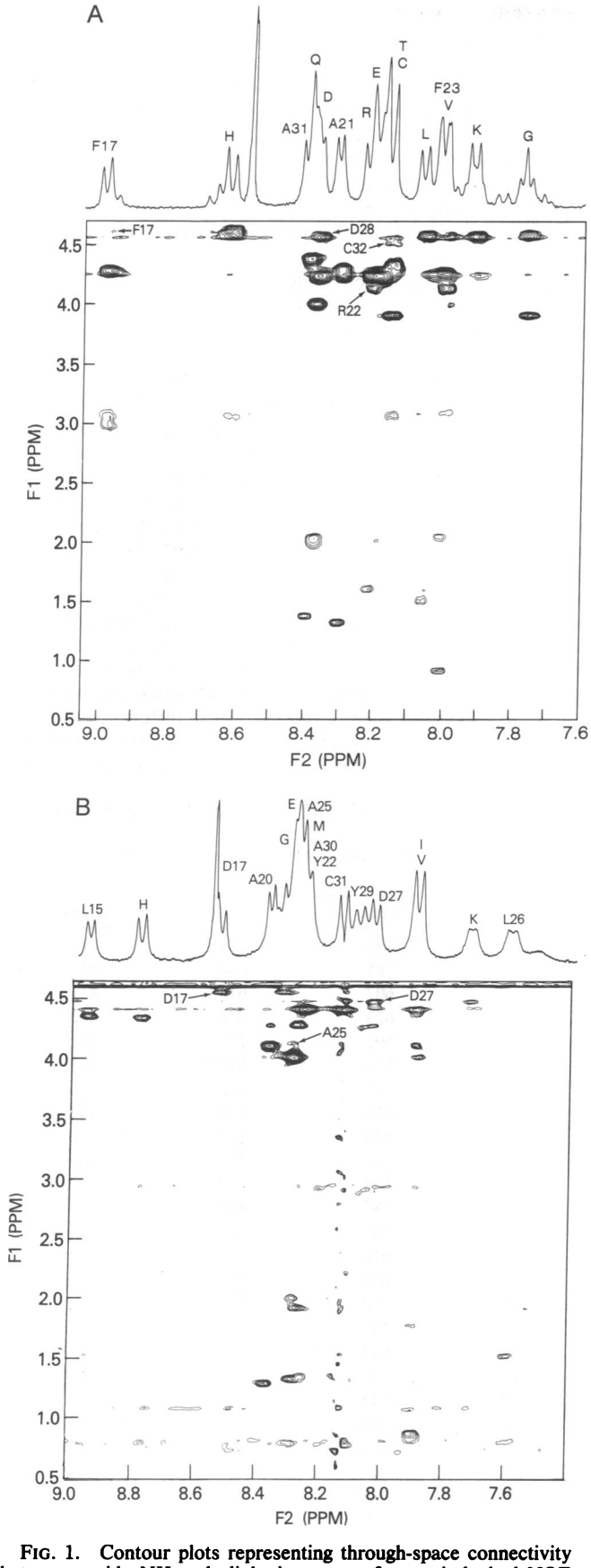

FIG. 1. Contour plots representing through-space connectivity between amide NH and aliphatic protons from spin-locked NOE spectra for 10 mM TB at pH 3.0 (*A*) and 4 mM EB at pH 3.14 (*B*). Solution conditions were 90% H_2O/10% ^2H_2O at 20°C. The mixing time was 120 ms in both cases. Labeled intraresidue cross peaks are used in the distance estimation process (4, 5).

protons, which are related to the short distances $d_{\alpha N}(i, i+1)$, provide most of the distance constraints. Throughout the text, the symbol $d_{AB}(i,j)$ is used as defined in ref. 12. The two spectra shown in Fig. 1 and other ROESY spectra with different mixing times do not show long-range NOEs between NH and aliphatic protons. However, the presence or absence of long-range NOEs involving aliphatic side chains, especially β and γ protons, is not clear because of severe overlap of the resonances associated with these protons. The cross-peak intensities are bracketed as strong, medium, and weak, corresponding to 2.2–2.4 Å, 2.4–2.6 Å, and 2.6–2.8 Å, respectively. The details of the procedures for relating cross-peak intensities to interproton distances have been described (4, 5).

Calculations are done in cartesian space by using both angular and distance restraints. The NOE-derived distances for the NH and α protons are converted to ψ and ϕ torsional angles before they are applied as restraints in the form of harmonic potentials. Ambiguities in the ϕ angles are eliminated by using $^3J(C^\alpha H—NH)$ vicinal coupling constants. The distances between the backbone protons (amide NH or $C^\alpha H$ protons) and side-chain protons (β, γ, etc.) are directly used as distance restraints and help in deciding the orientations of side-chain groups. Table 1 lists input distances for the simulations and the final output distances from the molecular dynamics trajectories.

Restrained Molecular Dynamics Simulations. The initial side-chain atom coordinates are randomly chosen from the parameter set PARAM19 (25) used in CHARMM (Chemistry at HARvard Molecular Mechanics). All energy minimization and restrained molecular dynamics calculations are performed with the GEMM (Generate, Emulate, and Manipulate Macromolecules) program (B.R.B., unpublished data) on a Star Technologies ST-100 array processor that is interfaced to an Apollo DN-590. The nonbonded cutoff is 8 Å, and 1-fs time steps are used. We first carried out thorough calculations for TB under a variety of conditions to find optimal conditions for the calculations, initially in "vacuum" and then in "water." In each case, three sets of simulations with differing NMR restraint force constants are used: (*i*) no NMR restraints, (*ii*) weak NMR restraining potentials with a force constant of 1.0 kcal/radians^2 (1 cal = 4.18 J), and (*iii*) strong NMR restraining potentials with a force constant of 200 kcal/radians^2. For calculations carried out in "water," a bag with 800 simulated water molecules with a radius of 19 Å is used. The potential energy for the "water" is calculated by using TIPS (transferable intermolecular potential functions) (26).

The energies of 25 initial structures with randomly selected dihedral angles are first minimized to eliminate any unreasonable forces due to the repulsive van der Waals contacts or to physically impossible geometries. These energy-minimized structures, which are then restrained by the NOE distances, are heated from 60 K to 600 K over a period of 10 ps and then allowed to undergo 35-ps molecular dynamics simulation at 600 K. Finally, the system is annealed to 300 K over 5 ps and allowed to undergo 40 ps of dynamics at 300 K. Details of the methodology and its corresponding implications will be the subject of a separate report.

RESULTS AND DISCUSSION

NMR spectroscopy is the method of choice for determining the three-dimensional solution structures of peptides. However, a number of factors such as precision in the estimate of the NOE values (27, 28), use of short interproton distances (≤4 Å), approximation of the rotational reorientation of the peptide in solution with a single correlation time model, and the internal mobility of the peptide chain (refs. 17, 29, and 30;

Table 1. Input and output interproton distances for molecular dynamics simulations for TB and EB in "water"

TB			EB		
Atoms	Input	Output	Atoms	Input	Output
F17NH-C16C$^{\alpha}$H	2.2	2.26	L15NH-C14C$^{\alpha}$H	2.2	2.18
F17NH-F17C$^{\alpha}$H	2.8	2.92	L15NH-L15C$^{\beta}$H	2.5	2.47
F17NH-F17C$^{\beta}$H	2.5	2.53	H16NH-L15C$^{\alpha}$H	2.2	2.14
H18NH-F17C$^{\alpha}$H	2.2	2.14	H16NH-H16C$^{\beta}$H	2.6	2.95
H18NH-H18C$^{\beta}$H	3.0	2.89	D17NH-H16C$^{\alpha}$H	2.5	2.32
G19NH-H18C$^{\alpha}$H	2.2	2.11	D17NH-D17C$^{\alpha}$H	2.2	2.15
G19NH-G19C$^{\alpha}$H	2.2	2.50	G18NH-D17C$^{\alpha}$H	2.3	2.15
T20NH-G19C$^{\alpha}$H	2.2	2.31	G18NH-G18C$^{\alpha}$H	>2.8	2.57
T20NH-A21NH	3.2	>3.50	V19NH-G18C$^{\alpha}$H	>2.8	3.08
T20NH-T20C$^{\gamma}$H	2.7	3.84	V19NH-V19C$^{\alpha}$H	2.4	2.75
A21NH-T20C$^{\alpha}$H	2.2	1.98	V19NH-V19C$^{\beta}$H	2.7	2.79
R22NH-A21C$^{\alpha}$H	2.2	2.27	A20NH-V19C$^{\alpha}$H	2.2	2.21
R22NH-R22C$^{\alpha}$H	2.5	2.87	A20NH-A20C$^{\beta}$H	2.6	2.76
R22NH-F23NH	3.2	>3.50	M21NH-A20C$^{\alpha}$H	2.2	2.08
R22NH-R22C$^{\gamma}$H	2.5	3.92	Y22NH-M21C$^{\alpha}$H	2.2	2.08
F23NH-R22C$^{\alpha}$H	2.2	2.08	Y22NH-Y22C$^{\alpha}$H	2.6	2.87
L24NH-R23C$^{\alpha}$H	2.2	2.01	Y22NH-Y22C$^{\beta}$H	2.7	2.90
L24NH-L24C$^{\beta}$H	2.5	2.57	I23NH-Y22C$^{\alpha}$H	2.2	2.20
L24NH-L24C$^{\gamma}$H	2.5	3.63	I23NH-I23C$^{\alpha}$H	2.5	2.72
V25NH-L24C$^{\alpha}$H	2.2	2.39	E24NH-I23C$^{\alpha}$H	2.2	2.04
V25NH-Q26NH	3.2	>3.50	A25NH-E24C$^{\alpha}$H	2.2	2.09
V25NH-V25C$^{\gamma}$H	3.0	3.61	A25NH-A25C$^{\alpha}$H	2.8	2.89
Q26NH-V25C$^{\alpha}$H	2.2	1.90	D26NH-A25C$^{\alpha}$H	>2.8	>3.50
Q26NH-Q26C$^{\beta}$H	2.5	2.35	D27NH-L26C$^{\alpha}$H	2.7	2.39
Q26NH-Q26C$^{\gamma}$H	3.0	3.54	D27NH-D27C$^{\alpha}$H	2.2	2.15
Q26NH-E27NH	3.2	>3.50	K28NH-D27C$^{\alpha}$H	2.5	2.46
E27NH-Q26C$^{\alpha}$H	2.2	2.22	Y29NH-K28C$^{\alpha}$H	2.7	2.58
E27NH-E27C$^{\beta}$H	2.7	2.69	A30NH-Y29C$^{\alpha}$H	ND	2.60
D28NH-E27C$^{\alpha}$H	2.2	2.02	C31NH-A30C$^{\alpha}$H	2.2	2.20
D28NH-D28C$^{\alpha}$H	2.3	2.15			
D28NH-K29NH	3.2	>3.50			
K29NH-D28C$^{\alpha}$H	2.2	2.12			
K29NH-K29C$^{\beta}$H	2.8	2.86			
K29C$^{\alpha}$H-P30C$^{\delta}$H	2.3	2.59*			
A31NH-P30C$^{\alpha}$H	2.2	2.23			
A31NH-A31C$^{\beta}$H	2.5	2.60			
C32NH-A31C$^{\alpha}$H	2.2	2.20			
C32NH-C32C$^{\alpha}$H	2.5	2.86			

Input distances (in Å) are those estimated from the ROESY experiments as described in refs. 4 and 5. Output distances are the averages of 25 and 24 final structures for TB and EB, respectively, after molecular dynamics simulations with strong restraints. The single-letter amino acid code is used. ND, not determined.

*The average for the trans conformers of proline only. The overall average, when the cis conformers are included in the averaging, is 3.57.

G. H. Weiss, J. E. Kiefer, and J.A.F., unpublished data) complicate the structure determination.

In the course of determining these structures, it seemed appropriate to consider some questions regarding the limitations of the method. Because of computational restrictions, most reported calculations have typically been performed in vacuum for short periods (<30 ps) (16, 17). Also, the initial structures used for some calculations do not differ significantly from the available x-ray structures in the case of proteins (19). The following questions thus arise. What is a sufficient trajectory simulation time? Does the final structure depend on the initial conditions? What is an appropriate criterion for convergence (i.e., minimized energy, root-mean-square deviation between computed and experimental interproton distances)? This latter question is important for peptides that are intrinsically more flexible than proteins. Finally, the influence of solvent on the structure is of critical importance (31).

As a result of our investigations on TB and EB, we are able to provide partial answers to some of these questions. The use of a high-speed array processor (ST-100) allows us to carry out simulations for 90 ps, which includes 45 ps of annealing (corresponding to ≈4 hr of computation time for each structure in "vacuum" and 12 hr in "water"). To the best of our knowledge, this study represents the first molecular dynamics simulation using NMR restraints that explicitly includes solvent molecules. Such inclusion of solvent addresses criticisms (31) that simulations in "vacuum" are not realistic.

Input for the restrained molecular dynamics simulations consisted of 25 energy-minimized structures. Both in "vacuum" and in "water," simulations of the energy-minimized structures using strong restraining potentials converge to pseudo-β-sheet structures. As expected, the use of strong restraints produced structures that are consistent with the experimental NMR distances. Simulations carried out in the absence of a restraining potential or with only a weak restraining potential did not give structures in accord with the experimental NMR distances. The associated energies are summarized in Tables 2 and 3. These are relative energies, whose zero is arbitrarily chosen in CHARMM. The contribution to the total energy from the restraining potentials has been subtracted from the final energies to permit comparison with different restraint constants. In "water" simulations, the water–water interaction energy is also subtracted. Simulations carried out in "vacuum" with strong restraints result in higher energy than those obtained with weak restraints or totally without restraints (Table 2). These differences (≈100 kcal/mol) originate from electrostatic interactions that are partially quenched by the solvent. It is important to note, however, that quantitative comparison of energies is only made within the "water" and within the "vacuum" simula-

Table 2. Relative energies of the simulated structures for TB in "vacuum"

Number	None	Weak	Strong
1	600	571	435
2	581	614	445
3	607	618	431
4	623	608	442
5	601	581	431
6	623	609	443
7	597	605	496
8	618	618	461
9	610	657	420
10	582	575	445
11	604	612	242
12	587	602	462
13	595	608	406
14	610	621	456
15	633	646	426
16	574	600	432
17	591	621	490
18	615	632	484
19	654	608	430
20	618	592	465
21	609	636	450
22	604	613	432
23	628	626	417
24	604	595	438
25	593	634	447
E_{av}	606 ± 18	612 ± 21	437 ± 46

The energies are expressed in units of kcal/mol and are negative relative to an arbitrarily chosen zero energy. None, weak, and strong represent the strength of the force constants (see text) associated with the restraint function used for the experimentally determined distances.

Table 3. Relative energies of the simulated structures for TB and EB in "water"

	TB							
	None		Weak		Strong		EB* strong	
Number	P	W	P	W	P	W	P	W
1	329	898	463	715	251	1081	372	1018
2	388	788	325	973	234	1135	315	1050
3	363	869	335	910	199	1157	357	986
4	360	793	394	847	125	1098	367	917
5	343	880	387	785	217	1121	293	1092
6	413	767	467	667	273	990	319	1017
7	364	832	343	898	254	982	385	966
8	419	741	165	825	254	1148	311	1111
9	251	929	168	545	180	1206	335	1086
10	319	930	343	861	230	1142	317	1060
11	386	796	300	957	272	1051	393	877
12	335	894	333	880	216	1077	275	1209
13	293	997	367	902	64	832	294	1130
14	397	814	361	904	253	1040	282	1135
15	386	825	140	738	256	1057	393	894
16	330	883	366	849	227	1106	248	1238
17	391	757	305	941	185	1208	373	968
18	349	880	146	694	201	1223	332	994
19	349	906	280	539	224	1121	358	997
20	399	843	372	879	219	1177	399	921
21	378	887	323	955	196	1098	257	1221
22	351	841	356	831	204	1135	300	1116
23	442	707	358	897	342	861	271	1217
24	402	837	413	769	275	1069	365	976
25	398	850	358	883	239	1106	—	—
E_{av}(P)	365 ± 42		327 ± 88		224 ± 53		330 ± 46	
E_{av}(W)	846 ± 67		826 ± 119		1089 ± 95		1050 ± 107	
E_{av}(P+W)	1211 ± 38		1152 ± 165		1312 ± 103		1379 ± 65	

The energies (E) are expressed in units of kcal/mol and are negative relative to an arbitrarily chosen zero energy. None, weak, and strong represent the strength of the force constant associated with the restraint function used for the experimentally determined distances. Columns P and W represent the energies associated with peptide–peptide and peptide–water interactions, respectively.
*For EB, only the strong restraints are used.

tions because of basic differences such as the dielectric constant.

In the "water" simulations, the average total energy, E_{av}(P+W) in Table 3, is significantly lower with strong restraints than when calculated with either weak restraints or no restraints. (The underlying assumption here is that the unweighted peptide–peptide and peptide–water energies in Table 3 are additive.) The E_{av}(P+W) value of the resulting

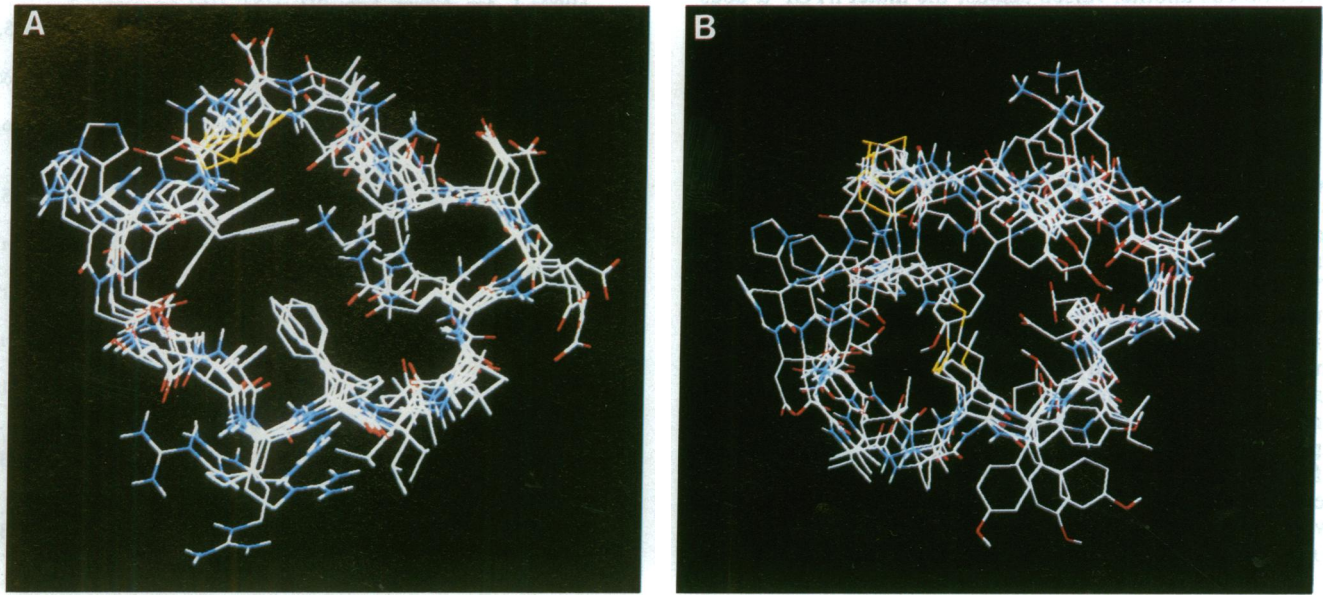

FIG. 2. Superpositions of the six lowest energy conformations of TB (*A*) and EB (*B*) obtained in "water" by using strong NMR restraints.

structures with strong restraints is −1312 kcal/mol, whereas the corresponding values for the cases with weak restraints and without restraints are −1152 kcal/mol and −1211 kcal/mol, respectively. The lower total energy obtained in the strong-restraint simulations results primarily from the water–peptide interaction (see Table 3).

Since the best results were obtained on TB with strong-restraint potentials in "water," calculations on EB are carried out only under these conditions. Table 3 summarizes the energies. Here E_{av}(P+W) is found to be −1379 kcal/mol.

Several explanations are possible for the dependencies of the final computed structures on the restraint potentials and the corresponding variations in energies of TB. One possibility is that only the simulations with strong restraints reach a global minimum energy during the 90-ps trajectories. Examination of the total energies at 5-ps intervals suggests convergence by 90 ps. Also, similarities in the energies and structures (see below) indicate that the final structures are independent of the initial conditions. Simulations using weak restraints appear to converge more slowly, although this behavior needs to be examined in more detail. In addition, the use of 25 random starting structures may not permit a complete examination of the conformational energy space in the time allotted.

The strong restraining potential was chosen to rapidly direct the trajectory toward the experimentally compatible structure. The value chosen for the restraining constant (200 kcal/rad^2) is arbitrary and eventually may be used to represent the precision in the estimate of the internuclear distances. The approximate nature of the potential functions used likely represents the most significant limitation of the computations.

In Fig. 2 is the superposition of the six lowest energy structures for TB and EB. For the most part, fluctuations around the side chains represent the significant differences in the various low-energy conformations.

Neither TB nor EB binds to the hEGF receptor (5). In fact, no single loop fragment from hEGF-related proteins is believed to bind. The conformations of the isolated fragments, TB and EB, do not differ appreciably from the conformations in the intact proteins (4, 5, 32, 33). It appears likely that the B loop could be important for receptor binding in the native protein when other contributing residues are present. Our preliminary antibody recognition study shows that a monoclonal antibody raised against the intact hEGF recognizes EB, whereas another raised against the intact hTGF-α does not recognize TB. The conformations of the putative recognition sites in TB and EB are significantly different (5) and may account for this behavior.

CONCLUSIONS

We have carried out NMR conformational analysis on the B-loop fragments of hTGF-α and hEGF, both in pseudo-vacuum and in the presence of surrounding simulated water molecules, using restrained molecular dynamics simulations. This study explicitly includes the effects of solvent molecules in molecular dynamics computations restrained by NOE distances by placing the peptides in a bag of 800 "water" molecules. In this study a large number of initial structures are generated for conformational determination of peptides and proteins by using the restrained molecular dynamics approach. A set of 25 randomly generated initial structures after 90-ps simulation under a strong NMR restraining potential yield a set of pseudo-β-sheet conformations, all of which are low in energy as well as consistent with the experimental NMR distance restraints only in the presence of the surrounding simulated water molecules. The results obtained here suggest that future computations must explicitly take into account the effects of the surrounding solvent molecules.

1. Robson, B. & Garnier, J. (1986) *Introduction to Proteins and Protein Engineering* (Elsevier, New York), Chap. 12.
2. Heath, W. F. & Merrifield, R. B. (1986) *Proc. Natl. Acad. Sci. USA* **83**, 6367–6371.
3. Appella, E., Robinson, E. A., Ullrich, S. J., Stoppelli, M. P., Corti, A., Cassani, G. & Blasi, F. (1987) *J. Biol. Chem.* **262**, 4437–4440.
4. Han, K.-H., Niu, C.-H., Roller, P. P. & Ferretti, J. A. (1988) *Biopolymers* **27**, 923–937.
5. Han, K.-H., Ferretti, J. A., Niu, C.-H., Lokeshwar, V., Clarke, R. & Katz, D. (1988) *J. Mol. Recognition* **1**, 116–123.
6. Bost, K. L., Smith, E. M. & Blalock, J. E. (1985) *Biochem. Biophys. Res. Commun.* **128**, 1373–1380.
7. Porter, R. & Whelan, J., eds. (1986) *Ciba Found.* Symp. **119**.
8. Kasier, E. T. & Kzedy, F. J. (1984) *Science* **223**, 249–255.
9. Fermi, G. & Perutz, M. F. (1981) in *Hemoglobin and Myoglobin: Atlas of Molecular Biology*, eds. Philips, D. C. & Richards, F. M. (Clarendon, Oxford).
10. Compton, L. A. & Johnson, W. C., Jr. (1986) *Anal. Biochem.* **155**, 155–167.
11. Brooks, B. R., Bruccoleri, R. E., Olafson, B. D., States, D. J., Swaminathan, S. & Karplus, M. (1983) *J. Comp. Chem.* **4**, 187–217.
12. Wuthrich, K. (1986) *NMR of Proteins and Nucleic Acids* (Wiley, New York).
13. Noggle, J. H. & Schirmer, R. E. (1971) *The Nuclear Overhauser Effect* (Academic, New York).
14. Sippl, M. J. & Scheraga, H. A. (1986) *Proc. Natl. Acad. Sci. USA* **83**, 2283–2287.
15. Billeter, M., Havel, T. F. & Wuthrich, K. (1987) *J. Comput. Chem.* **8**, 132–141.
16. Clore, G. M., Gronenborn, A. M., Brunger, A. T. & Karplus, M. (1985) *J. Mol. Biol.* **186**, 435–455.
17. Brunger, A. T., Clore, G. M., Gronenborn, A. M. & Karplus, M. (1987) *Protein Eng.* **1**, 399–406.
18. Brunger, A. T., Clore, G. M., Gronenborn, A. M. & Karplus, M. (1986) *Proc. Natl. Acad. Sci. USA* **83**, 3801–3805.
19. Nilges, M., Gronenborn, A. M., Brunger, A. T. & Clore, G. M. (1988) *Protein Eng.* **2**, 27–38.
20. van Gunsteren, W. F., Berendsen, H. J. C., Geursten, R. G. & Zwinderman, H. R. J. (1986) *Ann. N.Y. Acad. Sci.* **482**, 287–303.
21. Kruger, P., Strassburger, W., Wollmer, A. & van Gunsteren, W. F. (1985) *Eur. Biophys. J.* **13**, 77–88.
22. Mauger, A. B., Stuart, O. A., Ferretti, J. A. & Silverton, J. V. (1985) *J. Am. Chem. Soc.* **107**, 7154–7163.
23. Griesinger, C. & Ernst, R. R. (1987) *J. Magn. Reson.* **75**, 261–271.
24. Bothner-By, A. A., Stephens, R. L., Lee, J., Warren, C. D. & Jeanloz, R. W. (1985) *J. Am. Chem. Soc.* **106**, 811–813.
25. Reiher, W. E. (1984) Ph.D. Thesis (Harvard Univ., Cambridge, MA).
26. Jorgenson, W. L. (1981) *J. Am. Chem. Soc.* **103**, 335–340.
27. Weiss, G. H. & Ferretti, J. A. (1983) *J. Magn. Reson.* **55**, 397–407.
28. Weiss, G. H., Ferretti, J. A. & Byrd, R. A. (1987) *J. Magn. Reson.* **71**, 97–105.
29. Jelicks, L. A., Naider, F. R., Shenbagamurthi, P., Becker, J. M. & Broido, M. S. (1988) *Biopolymers* **27**, 431–449.
30. Wright, P. E., Dyson, H. J. & Lerner, R. A. (1988) *Biochemistry* **27**, 7167–7175.
31. Howard, A. E. & Kollman, P. A. (1988) *J. Med. Chem.* **31**, 1669–1675.
32. Montelione, G. T., Wuthrich, K., Nice, E. C., Burgess, A. W. & Scheraga, H. A. (1986) *Proc. Natl. Acad. Sci. USA* **83**, 8594–8598.
33. Cooke, R. M., Wilkinson, A. J., Baron, M., Pastore, A., Tappin, M. J., Campbell, I. D., Gregory, H. & Sheard, B. (1987) *Nature (London)* **327**, 339–341.